Determination of the Structure and Catalytic Mechanism of *Sorghum bicolor* Caffeic Acid *O*-Methyltransferase and the Structural Impact of Three *brown midrib12* Mutations[1][W]

Abigail R. Green, Kevin M. Lewis, John T. Barr, Jeffrey P. Jones, Fachuang Lu, John Ralph, Wilfred Vermerris, Scott E. Sattler, and ChulHee Kang*

School of Molecular Biosciences (A.R.G., C.K.) and Department of Chemistry (K.M.L., J.T.B., J.P.J., C.K.), Washington State University, Pullman, Washington 99164; Department of Biochemistry and Department of Energy Great Lakes Bioenergy Research Center, University of Wisconsin, Madison, Wisconsin 53726 (F.L., J.R.); Department of Microbiology and Cell Science and Genetics Institute, University of Florida, Gainesville, Florida 32610 (W.V.); and United States Department of Agriculture-Agricultural Research Service, Grain Forage and Bioenergy Research Unit, Lincoln, Nebraska 68583 (S.E.S.)

Using *S*-adenosyl-methionine as the methyl donor, caffeic acid *O*-methyltransferase from sorghum (*Sorghum bicolor*; SbCOMT) methylates the 5-hydroxyl group of its preferred substrate, 5-hydroxyconiferaldehyde. In order to determine the mechanism of SbCOMT and understand the observed reduction in the lignin syringyl-to-guaiacyl ratio of three *brown midrib12* mutants that carry *COMT* gene missense mutations, we determined the apo-form and *S*-adenosyl-methionine binary complex SbCOMT crystal structures and established the ternary complex structure with 5-hydroxyconiferaldehyde by molecular modeling. These structures revealed many features shared with monocot ryegrass (*Lolium perenne*) and dicot alfalfa (*Medicago sativa*) COMTs. SbCOMT steady-state kinetic and calorimetric data suggest a random bi-bi mechanism. Based on our structural, kinetic, and thermodynamic results, we propose that the observed reactivity hierarchy among 4,5-dihydroxy-3-methoxycinnamyl (and 3,4-dihydroxycinnamyl) aldehyde, alcohol, and acid substrates arises from the ability of the aldehyde to stabilize the anionic intermediate that results from deprotonation of the 5-hydroxyl group by histidine-267. Additionally, despite the presence of other phenylpropanoid substrates in vivo, sinapaldehyde is the preferential product, as demonstrated by its low K_m for 5-hydroxyconiferaldehyde. Unlike its acid and alcohol substrates, the aldehydes exhibit product inhibition, and we propose that this is due to nonproductive binding of the *S*-cis-form of the aldehydes inhibiting productive binding of the *S*-trans-form. The *S*-cis-aldehydes most likely act only as inhibitors, because the high rotational energy barrier around the 2-propenyl bond prevents *S*-trans-conversion, unlike alcohol substrates, whose low 2-propenyl bond rotational energy barrier enables rapid *S*-cis/*S*-trans-interconversion.

Lignin in plant cell walls confers structural support, provides a hydrophobic coating of xylem vessels to facilitate water transport through the vascular system, and protects against invading plant pathogens (Vanholme et al., 2010). Lignin is a complex polymer derived principally from monolignol (hydroxycinnamyl alcohol) precursors and related compounds. The three primary monolignols are coniferyl, sinapyl, and *p*-coumaryl alcohols, which give rise to guaiacyl (G), syringyl (S), and *p*-hydroxyphenyl subunits in polymerized lignin (Ralph et al., 2004; Vanholme et al., 2010). Due to its physical association with cellulose and physicochemical associations with hemicellulosic polysaccharides, and its ability to bind cellulolytic enzymes irreversibly, lignin is a major obstacle for the large-scale production of cellulosic biofuels and chemicals (Berlin et al., 2006; Dien et al., 2009; Ximenes et al., 2010). Thus, manipulation of the monolignol biosynthetic pathway is being pursued as a way to lower the energy cost and reduce the processing time associated with thermochemical pretreatment of the biomass (Chen and Dixon, 2007; Vermerris et al., 2007; Dien et al., 2009). This approach has the risk of depriving the plants of a crucial structural component that may well lead to weaker plants and reduced agronomic performance. Examples illustrating this risk include *brown midrib* (*bmr*) double mutants of forage sorghum (*Sorghum bicolor*; Pedersen et al., 2008), maize (*Zea mays*; Vermerris et al., 2010), and transgenic alfalfa (*Medicago sativa*) plants with reduced hydroxycinnamoyl-coenzyme A:shikimate hydroxycinnamoyl transferase

[1] This work was supported by the National Science Foundation (grant no. MCB 102114 to C.K.), the U.S. Department of Agriculture (National Research Initiative grant no. 35318–17454 to C.K.; Biomass Research and Development Initiative Competitive grant no. 2011–10006–30358 to W.V.; and grant nos. 5440–21220–032–00D and 2011–67009–30026 to S.E.S.), and by the Department of Energy Great Lakes Bioenergy Research Center (grant no. DE–FC02–07ER64494 to J.R. and F.L.).

* Address correspondence to chkang@wsu.edu.

The author responsible for distribution of materials integral to the findings presented in this article in accordance with the policy described in the Instructions for Authors (www.plantphysiol.org) is: ChulHee Kang (chkang@wsu.edu).

[W] The online version of this article contains Web-only data.

www.plantphysiol.org/cgi/doi/10.1104/pp.114.241729

(HCT; Shadle et al., 2007). Thus, the potential success or failure of metabolic engineering efforts aimed at improving biomass conversion hinges on a thorough understanding of the target pathway as it exists in the species of interest (Humphreys et al., 1999; Sarath et al., 2008; Vanholme et al., 2008; Walker et al., 2013).

Based on the current model of monolignol biosynthesis in angiosperms (Humphreys and Chapple, 2002), sinapyl alcohol is synthesized from precursors of guaiacyl residues, specifically coniferaldehyde and coniferyl alcohol, through the concerted action of the enzymes ferulate 5-hydroxylase (F5H) and caffeic acid *O*-methyltransferase (COMT). This model is based on kinetic studies with purified F5H from sweetgum (*Liquidambar styraciflua*; Osakabe et al., 1999) and Arabidopsis (*Arabidopsis thaliana*; Humphreys et al., 1999) that showed that F5H preferentially converted coniferaldehyde (Humphreys et al., 1999; Osakabe et al., 1999) and coniferyl alcohol (Humphreys et al., 1999) over ferulate. Consequently, coniferyl aldehyde/alcohol 5-hydroxylase is a more accurate name for this enzyme. COMT subsequently methylates the hydroxyl group on C5 of the phenolic ring.

This model is also consistent with the observed reduction in the proportion of S-residues in the lignin of Arabidopsis *fah1* mutants that carry mutations in the *F5H* gene (Meyer et al., 1996) and the marked increase in the proportion of S-residues that result from the overexpression of *F5H* (Meyer et al., 1998). The model is further supported by the observed reduction in the proportion of S-residues in plants in which *COMT* expression is down-regulated as the result of mutations or transgenic approaches (Chabbert et al., 1994; Atanassova et al., 1995; Van Doorsselaere et al., 1995; Guo et al., 2001; Bout and Vermerris, 2003; Marita et al., 2003; Fu et al., 2011; Jung et al., 2012; Sattler et al., 2012; Jung et al., 2013). In plants with reduced COMT activity, the low conversion of 5-hydroxyconiferaldehyde and 5-hydroxyconiferyl alcohol to the methylated derivatives leads to the incorporation of 5-hydroxyconiferyl alcohol into lignin, resulting in 5-hydroxyguaiacyl subunits in the polymer, as observed in maize *bm3* mutants (Lapierre et al., 1988; Marita et al., 2003) and sorghum *bmr12* mutants (Palmer et al., 2008). The incorporation of 5-hydroxyconiferyl alcohol into the growing lignin polymer also results in the formation of novel benzodioxane units (Ralph et al., 2001; Marita et al., 2003; Morreel et al., 2004).

Caffeoyl-coenzyme A *O*-methyltransferase (CCoAOMT) catalyzes the methylation reaction of caffeoyl-CoA to feruloyl-CoA (Martz et al., 1998), and this enzyme is thought to be responsible for the synthesis of the precursors of G-residues (Meng and Campbell, 1998). Down-regulation of CCoAOMT has indeed been shown to decrease G-lignin content in *Pinus radiata* (Wagner et al., 2011) and alfalfa (Guo et al., 2001). However, there are also data that potentially conflict with this model. In tobacco (*Nicotiana tabacum*), CCoAOMT has been shown to be able to methylate both 3- and 5-hydroxyl groups, with a strong preference for the thioester form of monolignol precursors (Martz et al., 1998). In alfalfa, COMT may be able to convert caffealdehyde to coniferaldehyde, suggesting some metabolic overlap between the biosynthetic routes toward precursors of G- and S-lignin (Parvathi et al., 2001). Furthermore, data on the effect of the down-regulation of *COMT* in alfalfa resulted in concomitant decreases in both G- and S-residues, again implicating COMT in the biosynthesis of coniferyl alcohol (Guo et al., 2001). The same was observed in transgenic ryegrass (*Lolium perenne*) in which the *LpOMT1* gene had been down-regulated. The S-G ratio of the lignin in the transgenic plant was unaltered relative to the untransformed controls (Louie et al., 2010; Tu et al., 2010). Some ryegrasses are polyploid, and the presence of diverged paralogous *OMT* genes could potentially compensate for the reduced *LpOMT1* expression. Alternatively, COMT in ryegrass may also play a role in the production of coniferaldehyde, so that its down-regulation would logically affect G-residues in the lignin, as proposed previously (Tu et al., 2010).

This study focuses on COMT in sorghum for two main reasons. First, sorghum, along with switchgrass (*Panicum virgatum*), has been proposed as an attractive herbaceous biofuel feedstock in the United States, due to its potential to produce large amounts of biomass, superior drought tolerance, and more efficient utilization of nitrogen-based fertilizers than many other crops, including the two main crops currently used for the production of biofuels there, maize and sugarcane (*Saccharum* spp.; Sarath et al., 2008; Vermerris and Saballos, 2012). The production of cellulosic biofuels from sorghum and switchgrass would translate to a lower environmental impact associated with biofuel production (Vermerris et al., 2007; Propheter and Staggenborg, 2010; Wortmann and Regassa, 2011).

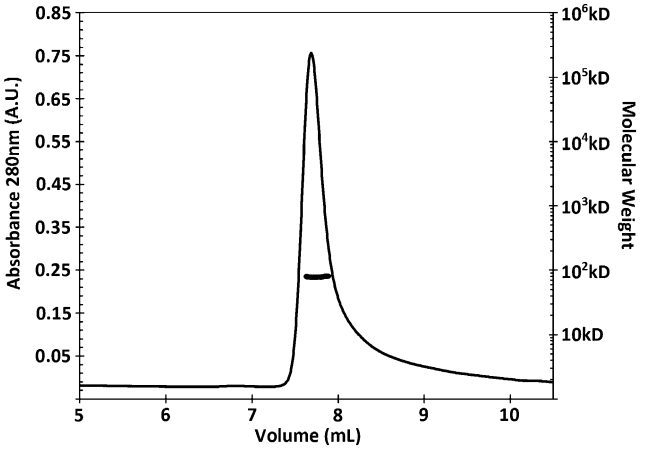

Figure 1. Molecular mass determination of SbCOMT. MALLS was performed using a 2 mg mL^{-1} SbCOMT solution. The chromatogram is shown as A_{280} (left *y* axis) and mass in kD (logarithmic; right *y* axis) versus elution volume (mL). The dots in the middle of the peak indicate the molecular mass (approximately 80 kD) calculated from the light scattering, indicating the dimeric nature of SbCOMT. A.U., Absorbance units.

Table I. *Crystallographic data for the SbCOMT apo and SAM cocrystal*

Data	Apo	SAM Complex
Wavelength (Å)	1.00	1.00
Resolution (Å)	50.0–2.1	50.0–2.8
Space group	$P2_12_12_1$	$P2_1$
Cell dimensions (Å)	a = 73.23	a = 76.65
	b = 96.29	b = 63.80
	c = 124.28	c = 152.32
	α = 90.00	α = 90.00
	β = 90.00	β = 93.07
	γ = 90.00	γ = 90.00
Asymmetric unit	2	4
Total observations	405,174	137,715
Unique reflections	58,703	36,802
Completeness (%)	99.4 (95.9)	99.6 (99.6)
R_{sym} [a,b]	0.083 (0.500)	0.060 (0.182)
Refinement		
Resolution (Å)	38.1–2.1	37.5–2.8
No. of reflections	58,312	36,655
R_{cryst} [c]	0.1899	0.2158
R_{free} [d]	0.2281	0.2567
Root mean square distance bonds (Å)	0.009	0.002
Root mean square distance angles (°)	1.472	0.480
No. of atoms		
Protein and ligand	5,817	10,537
Water	360	47

[a]Numbers in parentheses refer to the highest resolution shell. [b]$R_{sym} = \Sigma I_h - <I_h>|/\Sigma I_h$, where $<I_h>$ is the average intensity over symmetry equivalent reflections. [c]$R_{cryst} = \Sigma||F_{obs}| - |F_{calc}||/\Sigma|F_{obs}|$, where summation is over the data used for refinement. [d]R_{free} was calculated as for R_{cryst} using 5% of the data that was excluded from refinement.

Second, several *bmr12* mutants with reduced COMT activity have been identified in sorghum (Bout and Vermerris, 2003; Saballos et al., 2008; Sattler et al., 2012). Because of their reduced lignin content and altered lignin subunit composition, they are promising as biomass feedstocks for biofuel production (Vermerris et al., 2007; Saballos et al., 2008; Dien et al., 2009; Sattler et al., 2010, 2012), but they are also of value to study the catalytic mechanism of COMT in this species. This will enable the elucidation of the main role of this enzyme and can form the basis of future protein engineering approaches to modify cell wall composition. Based on the genomic sequence of sorghum (Paterson et al., 2009), it possesses only a single gene encoding a functional *S*-adenosyl-L-methionine (SAM)-dependent COMT, making sorghum COMT (SbCOMT) an ideal candidate for the effective manipulation of monolignol biosynthesis (Bout and Vermerris, 2003; Sattler et al., 2012).

We present here a range of data elucidated for SbCOMT, including crystal structures and thermodynamic and kinetic data, to gain a mechanistic understanding of this key enzyme and to enable future manipulation of the monolignol biosynthesis and lignin content of sorghum.

RESULTS

Determination of Its Global Structure Establishes That SbCOMT Forms a Dimer

Several analyses were performed to obtain information on the global structure of SbCOMT. Multiangle laser light scattering (MALLS) of SbCOMT in solution revealed the molecular mass to be 80 kD (Fig. 1), twice the expected mass calculated from the monomeric SbCOMT amino acid sequence, indicating that this enzyme forms a dimer. Next, detailed structural analyses were performed on the crystallized apo-form and the SAM binary complex proteins. The apo-form SbCOMT crystallized in the orthorhombic space group, $P2_12_12_1$, with two molecules in the asymmetric unit. This crystal packing was consistent with the MALLS data. The refined model at 2.1 Å resolution of apo-form SbCOMT had an R_{work} of 17.50% and R_{free} (for free R-factor) of 21.5%. On the other hand, the SbCOMT enzyme that had been preincubated with SAM crystallized in the monoclinic space group, $P2_1$, with four molecules in the asymmetric unit that maintained the same type of dimer interaction. The detailed crystallographic data for the native apo-form and the SAM binary

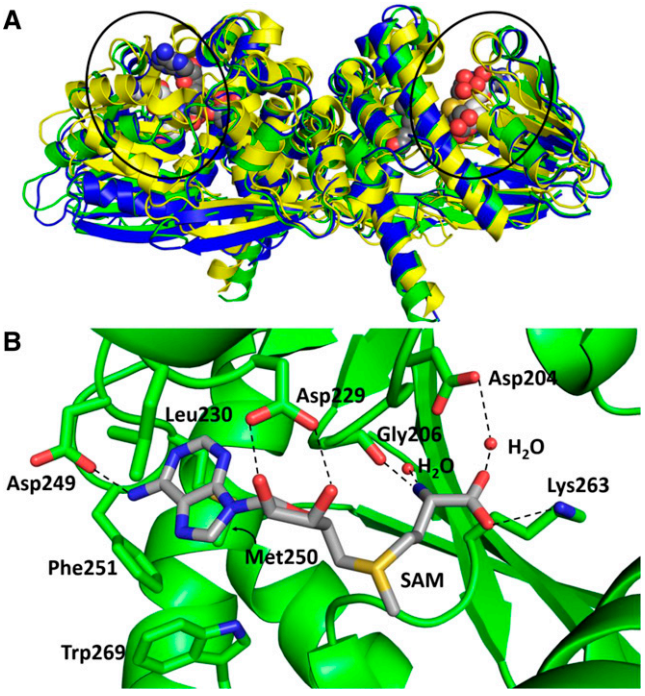

Figure 2. Domain shifts of SbCOMT. A, Cα least-squares superposition of apo-SbCOMT (blue), its SAM complex (green), and LpCOMT (yellow) to illustrate bound substrate-induced domain shifts. SAM in the SbCOMT active site is shown as light-gray spheres for carbons, blue spheres for nitrogen atoms, and red spheres for oxygen atoms; the coloration for SAH and sinapaldehyde in the LpCOMT active site are the same except that dark-gray spheres represent carbons. B, Closeup of the SbCOMT active site with bound SAM. Amino acid residues are labeled, and hydrogen bonds between residue side chains and SAM are shown as black dashed lines. These images were generated using the PyMOL Molecular Graphics System, version 1.3 (Schrödinger).

complex of SbCOMT (2.8 Å) are reported in Table I. The refined structures of each of the subunits in both the apo-form and the binary complex showed very low levels of electron density for the five residues at the N termini, reflecting their disordered nature. The root mean square distance between the Cα positions of the apo-form and the SAM binary complex was 0.83 Å, showing that the overall structures were very similar, as is evident from the superimposed structures (Fig. 2).

Each individual subunit contained nine β-strands and 16 α-helices (Fig. 3). Although the two domains were not fully separated in terms of their primary structure, each enzyme consisted of a Rossmann-like fold SAM-binding domain and a phenylpropanoid-binding domain, a part of which also constituted the dimer interface. Those two subunit molecules were tightly intertwined at the dimer interface, with their enzyme active sites facing the same direction parallel to the dimer interface and toward the outer edge of the dimer (Fig. 4). The dimer interface consisted mainly of α1 (residues 11–39), which lay in a cleft of the adjacent subunit and established numerous polar and hydrophobic contacts with every other subunit. Additional contributions from α4, α6, α15, and α16 established the cleft in which α1 could intertwine. In particular, there was a ball-and-socket type of interaction, in which His-314 (α15) of one monomer was hydrogen bonded on both nitrogen atoms of its imidazole group by Ser-25 (α1) and Tyr-85 (α4) of the other subunits. Additional polar contacts that secured both the α1 interactions and the twisted β-sheet of the dimer interface included Asp-13 to Lys-110, Glu-14 to Tyr-330, Tyr-19 to the backbone carbonyl of Tyr-85, Nδ of Asn-35 to the backbone carbonyl of Trp-137, Asp-73 to Arg-327, and Ser-84 to Gln-310. In addition, several hydrophobic interactions

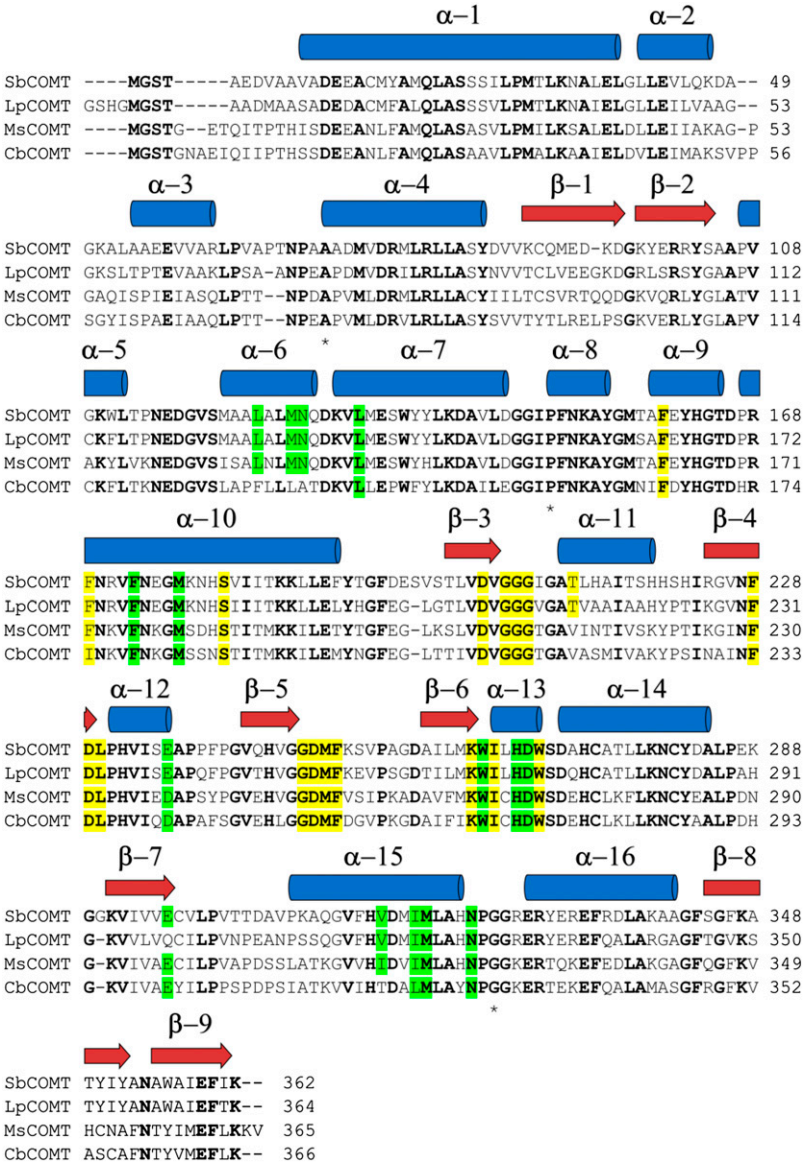

Figure 3. Multiple sequence alignment of COMTs from sorghum (SbCOMT), ryegrass (LpCOMT), alfalfa (MsCOMT), and *C. breweri* (CbCOMT). The α-helices and β-strands of SbCOMT are depicted with blue tubes and pink arrows, respectively. The SAM- and phenylpropanoid-binding residues are indicated by yellow and green highlights, respectively, and the identical residues among the compared sequences are in boldface. Asterisks indicate the locations of point mutations observed in sorghum *bmr12* mutants. Multiple sequence alignment was performed with ClustalW using a BLOSUM weighting matrix.

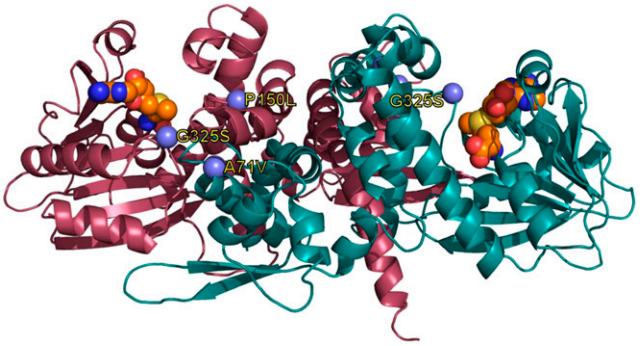

Figure 4. Ribbon diagram representing the crystal structure of SbCOMT with bound SAM. The SbCOMT dimer is displayed as a ribbon diagram with bound SAM (orange spheres). The positions of the point mutations in the *bmr12* mutants are shown as light-blue spheres. This image was generated using the PyMOL Molecular Graphics System, version 1.3 (Schrödinger).

were found at this dimer interface, including dispersion interactions between the thiol of Cys-17 and the indole ring of Trp-111. Overall, those observed interactions between the two subunits established a stable dimer in solution, consistent with the MALLS data (Fig. 1).

Characterization of the Substrate-Binding Pockets

C-Terminal SAM-Binding Pocket

In the binary complex of SbCOMT, the SAM molecule was bound by the loops in the smaller $\beta\alpha\beta\alpha\beta$ motif with a conformation that is common to class I methyltransferases (Figs. 3 and 4). The methionyl chain of the bound SAM was in an extended trans position from the ribosyl moiety, secured by both hydrogen bonds and hydrophobic interactions. The SAM carboxylate established hydrogen bonds to Nζ of Lys-263, and its amino group formed hydrogen bonds to the backbone carbonyls of Gly-206 and Lys-263, as well as Val-205, via a bound water molecule. In addition, the SAM methionyl side chain was stabilized by hydrophobic interaction with the side chain of nearby Ile-265 (Fig. 3). The 3′ and 4′ ribosyl hydroxyl groups were within hydrogen bonding distance of the carboxylate of Asp-229. The SAM adenosyl ring was also secured by hydrophobic interactions. The side chains of Leu-230 and Met-250 established dispersion interactions on either face of the adenine base. Additionally, Phe-228, Phe-251, and Trp-269 formed the rest of the hydrophobic pocket, with favorable edge-to-face interactions with the adenine base. Finally, the 6′ adenosyl amino group was hydrogen bonded to the carboxylate of Asp-249.

5-Hydroxyconiferaldehyde-Binding Pocket

The pocket was surrounded by five α-helices, including one that originated from the dimeric partner that plugs one side of the pocket without providing any closely interacting residues to the modeled 5-hydroxyconiferaldehyde. In detail, the binding pocket was established by Leu-124, Met-127, Asn-128, and Leu-133 from α6 and α7, Phe-173 and Met-177 from α10, Trp-264, His-267, and Asp-268 from α13, and Val-315, Ile-318, Met-319, and Asn-323 from α15 (Fig. 3). Overall, most of the constituting residues are nonpolar, except for Asn-128, His-267, Asp-268, and Asn-321. The 5-hydroxyl group of the modeled 5-hydroxyconiferaldehyde was within a hydrogen bond distance from both the carboxyl side chain of Asp-268 and the imidazole Nε atom of His-267. The Nδ atom of this residue, in turn, was hydrogen bonded to the carboxyl side chain of Glu-328. In addition, the carboxyl side chain of Glu-296 was located close enough to produce an electrostatic effect to the same imidazole ring of His-267.

SbCOMT Has Affinity for Multiple Phenylpropanoid Compounds

Isothermal titration calorimetry (ITC) measurements were performed to compare the differential binding affinities between SAM and *S*-adenosylhomocysteine (SAH), the product formed following the removal of the methyl group from SAM. Titration curves for SAH and SAM were obtained at both pH 6.5 (Fig. 5A) and pH 7.5 (Fig. 5B). The resulting dissociation constant (K_d) values at pH 6.5 for SAH and SAM were 5 ± 2 μM and 13 ± 2 μM, respectively. At pH 7.5, the binding of SAM was approximately the same, 13 ± 1.3 μM, but the SAH binding was tighter at 1.9 ± 0.3 μM.

The K_d values of *p*-coumaraldehyde, coniferaldehyde, 5-hydroxyconiferaldehyde, and caffeic acid were 160, 36, 1.8, and 11 μM, respectively. The ITC data indicated a substantial entropic contribution to the binding of most of these compounds (Table II; Fig. 5). Ferulic acid, sinapic acid, sinapaldehyde, and caffeyl alcohol also displayed significant affinity for SbCOMT (data not shown), but severe protein precipitation occurred in every case right before ligand saturation, preventing the interpretation of thermograms due to the substantial amount of heat released upon the precipitation of SbCOMT. On the other hand, the titration curves of caffeoyl-CoA (Fig. 5C, circles), cinnamic acid (Fig. 5C, triangles), and cinnamaldehyde (Fig. 5D, diamonds) indicated that SbCOMT did not have any significant affinity for these compounds.

Determination of Steady-State Kinetics Identifies 5-Hydroxyconiferaldehyde as the Preferred Substrate and as an Inhibitor

Given that the lowest K_d values measured among the phenylpropanoid substrates were those for 5-hydroxyconiferaldehyde and caffeic acid, their kinetic curves were determined, along with those for the methyl donor SAM (Fig. 6). As substrate inhibition for aldehyde substrates had been observed previously in LpCOMT at pH 7.5

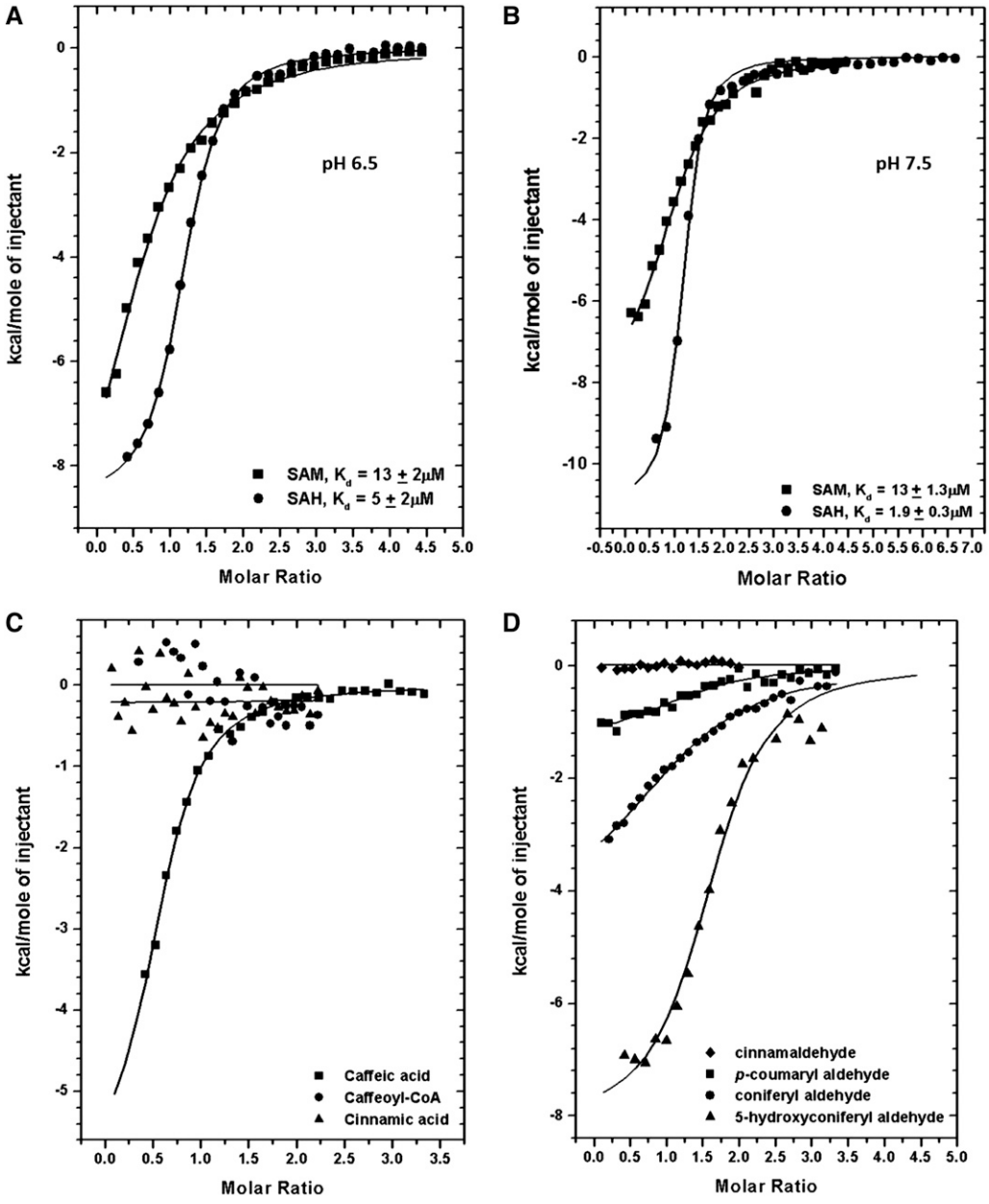

Figure 5. Measurement of SbCOMT substrate binding through ITC experiments. A and B, Trend of heat released by serial injections of SAM (squares) and SAH (circles) at pH 6.5 (A) and pH 7.5 (B). C, Trend of heat released by serial injections of caffeoyl CoA (circles), cinnamic acid (triangles), and caffeic acid (squares). D, Trend of heat released by serial injections of cinnamaldehyde (diamonds), *p*-coumaraldehyde (squares), coniferaldehyde (circles), and 5-hydroxyconiferaldehyde (triangles). Solid lines represent the least-square fits of the data.

(Louie et al., 2010), 5-hydroxyconiferaldehyde kinetic curves for SbCOMT were obtained at both pH 7.5 and 6.5. At both pH values, the decreased initial velocity at higher 5-hydroxyconiferaldehyde concentrations indicated that SbCOMT, like LpCOMT, is sensitive to substrate inhibition. The resulting K_m and turnover number (k_{cat}) of SbCOMT for 5-hydroxyconiferaldehyde at pH 7.5 were 1.1 ± 0.4 μM and 5.3 ± 1.2 μkat mg^{-1} SbCOMT, respectively. At pH 6.5, the K_m and k_{cat} were 0.86 ± 0.3 μM and 5.9 ± 1.0 μkat mg^{-1}, respectively. Although these numbers are quite similar, the observed inhibition constant (K_i) values at pH 7.5 and 6.5 differed substantially at 2.7 ± 1.1 μM and 10 ± 4.8 μM, respectively (Table III; Fig. 6A), indicating that at pH 6.5, 5-hydroxyconiferaldehyde is a less potent inhibitor than at physiological pH. For caffeic acid, the K_m and k_{cat} were 12 ± 2.5 μM and 7.5 ± 0.5 μkat mg^{-1} (Table III; Fig. 6B). Finally, the K_m and k_{cat} for SAM were determined as 17 ± 2.4 μM and 4.9 ± 0.2 μkat mg^{-1} (Table III; Fig. 6C). No evidence of substrate inhibition was identified for either caffeic acid or SAM.

Table II. *Thermodynamic parameters for binding of phenylpropanoids*

Phenylpropanoid	K_d	Enthalpy Change	Entropy Change
	μM	*kcal mol*$^{-1}$	*cal mol*$^{-1}$ *K*$^{-1}$
p-Coumaraldehyde	160 ± 80	−2.1 ± 0.2	6.9
Coniferaldehyde	36 ± 4	−3.9 ± 0.2	7.4
5-Hydroxyconiferaldehyde	1.8 ± 0.2	−5.9 ± 0.08	6.4
Caffeic acid	11 ± 1.3	−6.2 ± 0.5	1.8

The lower K_m values for 5-hydroxyconiferaldehyde relative to caffeic acid indicate that the former substrate is preferred when both substrates are present.

Substrates and Products Interact with SbCOMT following a Rapid Equilibrium Random Mechanism

In order to determine the sequence in which the SAM and phenylpropanoid substrates bind, enzyme kinetics were determined using combinations of different concentrations of both substrates. Analysis of the resulting data using Lineweaver-Burk plots was then able to identify the enzyme mechanism of SbCOMT. Furthermore, product inhibition studies were applied to determine whether the corresponding inhibition is competitive or noncompetitive. This analysis was complicated by the fact that 5-hydroxyconiferaldehyde showed substrate inhibition (Fig. 6A). Hence, caffeic acid was used to investigate the sequential binding mechanism of SbCOMT, because this substrate did not show any inhibitory effect on SbCOMT enzymatic activity. SbCOMT's initial velocities with respect to SAM at varying caffeic acid concentrations, as well as SbCOMT's initial velocities with respect to caffeic acid at varying SAM concentrations, demonstrated that the mechanism was sequential rather than ping-pong (Fig. 7, A and B). Additionally, product inhibition by SAH was noncompetitive with respect to caffeic acid (Fig. 7C) but competitive with respect to SAM (Fig. 7D). Product inhibition by ferulic acid was competitive with respect to both caffeic acid and SAM (Fig. 7, E and F). Taken together, these data suggest a rapid equilibrium random mechanism with a caffeic acid:SAH dead-end complex (Fig. 7G). In essence, either SAM or caffeic acid binds to the apo-form SbCOMT, and once both are bound, the resulting complex can then be converted into products that are released in no specific order. Caffeic acid can also bind to the SbCOMT:SAH complex.

The Impact of *bmr12* Mutations on the Secondary Structure of SbCOMT

In order to further examine the effects on the secondary structure of SbCOMT that result from four *bmr12* mutations described previously (Sattler et al., 2012), the corresponding mutant enzymes were generated via site-directed mutagenesis and expressed in *Escherichia coli*. The *bmr12* missense mutants were Ala-71Val, Pro-150Leu, Gly-325Ser, and Ala-71Val:Pro-150Leu, a double mutant. The mutated recombinant proteins were purified via affinity chromatography and characterized using circular dichroism (CD). The shape and intensity for the far UV light-CD spectra of the Ala-71Val and Gly-325Ser mutants were similar to what was observed for the wild-type protein, indicating that they contain a similar amount of secondary structure (Fig. 8). However, both single and double mutants of Pro-150Leu displayed significantly changed CD patterns, indicative of substantial changes in secondary structure.

The High Free Rotational Energy Barrier of 5-Hydroxyconiferaldehyde May Explain the Substrate Inhibition by This Compound

A possible explanation for the substrate inhibition of SbCOMT by 5-hydroxyconiferaldehyde is the ability of this substrate to bind with the 5-hydroxyl group in one of two orientations that are dictated by the relative dihedral conformation of the propenal side chain. In order to examine the ease with which 5-hydroxyconiferaldehyde can alternate between these two conformations, the rotational energy barriers were determined via density functional theory calculations. This analysis shows that rotation around the C_7-C_8-C_9-O dihedral angle is a facile process for 5-hydroxyferulate and 5-hydroxyconiferyl alcohol, but that a high energetic barrier (ΔE [change in energy of the system]) of 11 kcal mol^{-1} exists for that rotation in 5-hydroxyconiferaldehyde. Free energy analysis shows that the free energy change (ΔG) between the *S*-cis- and *S*-trans-states is 2.76 kcal mol^{-1}.

DISCUSSION

To identify SbCOMT homologs, a comparison of the determined structures of SbCOMT with available structures in the Protein Data Bank (PDB) was carried out using a Dali search (Holm and Sander, 1993). The most similar structure was a ryegrass COMT (PDB identifier 3P9C; Louie et al., 2010) with a high *Z* score of 46.3, followed by an alfalfa COMT (PDB identifier 1XYW; Zubieta et al., 2002) and a *Clarkia breweri* COMT (PDB identifier 3REO) with *Z* scores of 43.8 and 41.5, respectively. A BLAST (Altschul et al., 1997) search of the PDB also revealed that those three COMTs have the highest sequence identity with SbCOMT, at 77%, 61%, and 54%, respectively. The sequence identity of MsCOMT with CbCOMT, both dicot COMTs, is 71%, which is higher than the sequence identity with either SbCOMT or LpCOMT. Sequence alignment

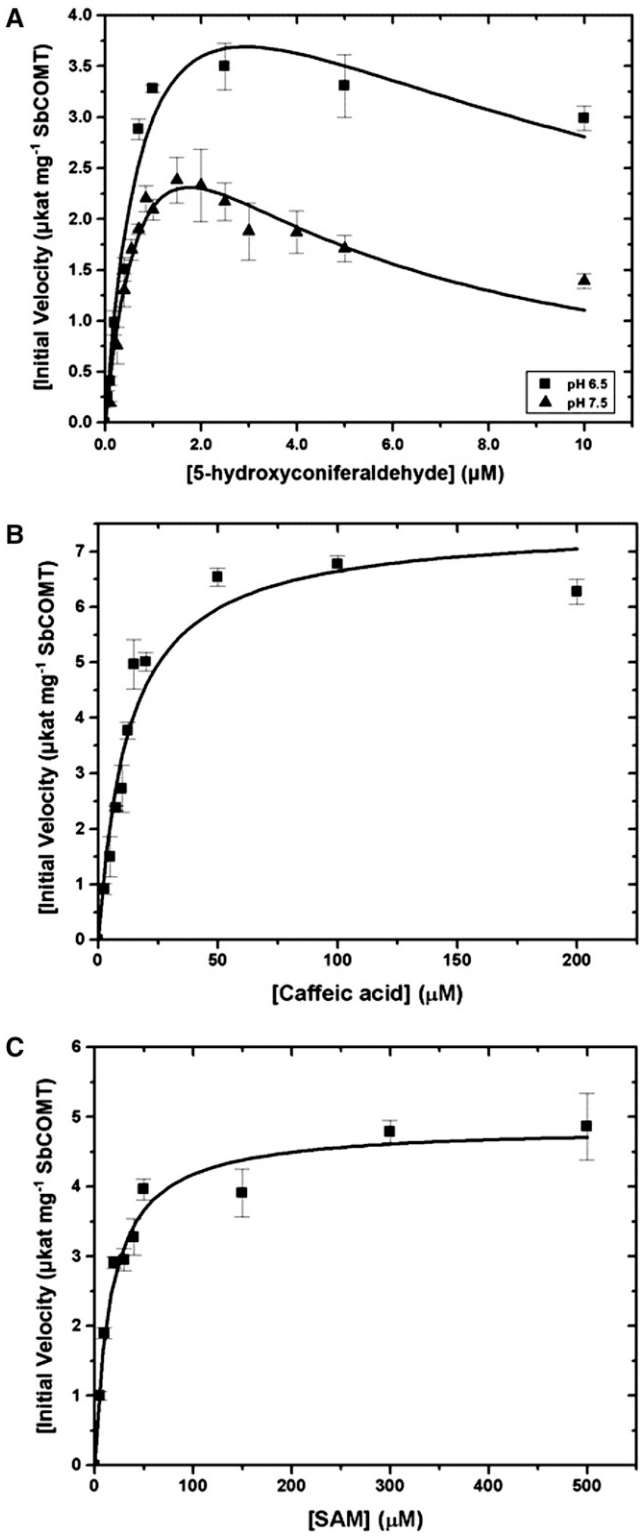

Figure 6. Kinetic activity of SbCOMT. A, Kinetic curve of SbCOMT reacting with varying concentrations of 5-hydroxyconiferaldehyde at pH 6.5 (squares) and pH 7.5 (triangles). B and C, Kinetic curves of SbCOMT with varying concentrations of caffeic acid (B) or SAM (C).

also revealed that the residues constituting the binding pockets for both substrates are more conserved between SbCOMT and LpCOMT (Fig. 3).

Motion in SbCOMT

The apo-form SbCOMT structure was in the open conformation, and a small amount of domain closure was noticed upon SAM association (Fig. 2). However, full closure, as observed in the ternary complex structure of COMT from ryegrass (Louie et al., 2010), is required to bring the methylsulfonium of SAM into close proximity with the 5-hydroxyl moiety of 5-hydroxyconiferaldehyde for catalysis (Fig. 2). Considering that our ITC data show significant affinity of the apo-form of SbCOMT with 5-hydroxyconiferaldehyde (Fig. 5D) and considering the configuration of the side chains constituting the binding pocket for 5-hydroxyconiferaldehyde observed in the SAM binary complex structure, only the open form will be able to accommodate the binding of 5-hydroxyconiferaldehyde. Due to its blocked nature, it is unlikely that substrates can diffuse into the closed conformation. Thus, in the open state, either SAM or 5-hydroxyconiferaldehyde binds to its corresponding pocket. Upon binding of both substrates, it is likely that the enzyme is either locked up in a closed conformation or has a greatly slowed open-closure motion, which is consistent with the random bi-bi mechanism (Fig. 7G). To analyze the structural changes that lead to the closed form of the active enzyme, the absolute differences between the LpCOMT open- and closed-form Ψ and Φ dihedral angles were plotted versus residue number (Supplemental Fig. S1). The largest differences were found in the α-helical region between Pro-150 and Pro-167 and in a disordered loop region between Pro-298 and Pro-305, the latter region containing the top three differences: $|\Delta\Psi| = 169.2$ for Val-299, $|\Delta\Phi| = 155.4$ for Asn-300, and $|\Delta\Psi| = 89.8$ for Pro-301. With the Ψ and Φ angles changed for residues 298 to 305, the protein experienced a major domain shift that helped close the protein. However, the biggest change in closing the active site occurred by changing Ψ and Φ for Phe-160 and Gly-164, which had the overall effect of closing off the ligand entry site and is most likely accompanied by a loss of solvent from the active site. One of the *bmr12* missense mutations resulted in a change of Pro-150 to Leu-150; the ensuing severe reduction in enzyme activity is consistent with the importance of the region between residues 150 and 167 for enzyme closure.

Catalytic Reaction Mechanism and Substrate Specificity

Based on the analysis of a combination of data and modeling, it is possible to propose a plausible catalytic mechanism for SbCOMT. The modeled 5-hydroxyconiferaldehyde was snuggly bound in the expected pocket through hydrogen bonding and hydrophobic interactions (Fig. 9). In addition, all of the tested phenylpropanoids (Supplemental Fig. S2) were able to dock

Table III. *Kinetic parameters for SbCOMT substrates*

n/a, Not applicable.

Substrate	k_{cat}	K_m	K_i
	$\mu kat\ mg^{-1}$	μM	μM
5-Hydroxyconiferaldehyde, pH 6.5	5.9 ± 1.0	0.86 ± 0.30	10 ± 4.8
5-Hydroxyconiferaldehyde, pH 7.5	5.3 ± 1.2	1.1 ± 0.4	2.7 ± 1.1
Caffeic acid	7.5 ± 0.5	12 ± 2.5	n/a
SAM	4.9 ± 0.2	17 ± 2.4	n/a

into the same pocket. Hydrogen bonds were implicated between the 5-hydroxyl group of 5-hydroxyconiferaldehyde and Nε of His-267, between the 4-hydroxyl group and Asp-268, and a water-mediated hydrogen bond between the 4-hydroxyl group and Oδ of Asn-323. The imidazole ring of His-267 was in close proximity with carboxyl side chains of Glu-296 and Asp-268, which could electrostatically increase its ability to abstract acidic protons.

Upon binding, the hydrogen atoms at the 4- and 5-hydroxyl groups of 5-hydroxyconiferaldehyde reorient themselves, as proposed in LpCOMT, from the more favorable *syn*-conformation to an *anti*-conformation, with respect to the *S*-trans-aldehyde, through electrostatic attraction by Asp-268; consequently, the 5-hydroxyl hydrogen is oriented toward His-267. Here, the 5-hydroxyl group can be deprotonated to form an imidazolium that is stabilized by Glu-328. The 5-phenolate substrate generated by this acid-base catalysis is then methylated by SAM to give sinapaldehyde and SAH (Fig. 10). Once SbCOMT returns to its open form and releases sinapaldehyde and SAH, a bound water molecule connected to bulk solvent is able to deprotonate His-267, thereby regenerating the catalytic base form of His-267 (Fig. 10).

Substrate Specificity

The size of the phenylpropanoid-binding pocket was rather big in SbCOMT (Fig. 9) and other known COMT structures of different species and thus could accommodate various aldehydic, alcoholic, and carboxylic acid compounds. A previous study (Louie et al., 2010) showed that recombinant SbCOMT efficiently utilized four tested phenolic substrates: caffeic acid, caffeyl alcohol, 3,4-dihydroxybenzaldehyde, and 3,4-dihydroxy-5-methoxybenzaldehyde. Among those tested compounds, 3,4-dihydroxy-5-methoxybenzaldehyde displayed the highest affinity (K_m = 4.5 μM) and 3,4-dihydoxybenzaldehyde the lowest affinity (K_m = 38.0 μM), indicating that the presence of a methoxyl group contributed to increased affinity. In addition, the thermodynamic parameters upon the association of *p*-coumaraldehyde, coniferaldehyde, and 5-hydroxyconiferaldehyde indicated that the corresponding affinity increased with each substituent added to the C3 and C5 positions (Table II). Considering our ITC data (Fig. 5, C and D; Table II) and the hydrophobic nature of the binding pocket (Fig. 9), a substantial portion of the binding of those compounds and other phenylpropanoids is contributed by an entropy gain from released water.

Although SbCOMT displayed a high k_{cat}/K_m when reacting with 5-hydroxyconiferaldehyde, it also exhibited substantial substrate inhibition at high concentrations (Fig. 6A). Caffeic acid, on the other hand, did not show any substrate inhibition, despite being a relatively poor substrate (Fig. 6B). In addition, LpCOMT displays similar substrate inhibition to both 5-hydroxyconiferaldehyde and caffealdehyde, but no inhibition by caffeic acid, caffeyl alcohol, and 5-hydroxyferulic acid was observed (Louie et al., 2010). Therefore, it is tempting to speculate that this inhibition is unique to aldehydic phenylpropanoids. If that is the case, the noticeable inhibition is likely due to the rotational barrier of the aldehydic portion of the substrate, which does not exist in the alcoholic and carboxylic acid counterparts (Fig. 11). The energy barrier, which was observed in trans-cinnamaldehyde, results in a significant portion being in the *S*-cis-configuration (Egawa et al., 2008). The *S*-cis-form can establish an analogous hydrogen bond with Asn-128, but this nonproductive binding could cause the observed competitive inhibition (Fig. 10B). Supporting this notion, such nonproductive binding can be envisioned from the noticeable electron density for an alternate coniferaldehyde methoxyl group conformation, one in which the methoxyl group is pointed away from SAH, in the difference map at coniferaldehyde of the deposited LpCOMT structure (PDB identifier 3P9K). Crystallographic occupancy refinement of this alternate conformer estimated that approximately 40% of coniferaldehydes are bound in the active site with their methoxyl groups facing away from SAH, which shows that coniferyl substrates, and thus 5-hydroxyconiferyl substrates, can bind with their methoxyl groups in either orientation, consistent with our hypothesis on the mechanism for substrate inhibition.

Enzymatic Activity toward Substrates Containing Aldehyde, Alcohol, and Carboxylic Acid Functional Groups on the Propenyl Chain

The preference of MsCOMT for aldehydes over the alcohols and free acids was reported previously (Zubieta et al., 2002). Considering all other published data, a consistent trend exists for compounds that contain the same phenyl substitutions: COMT prefers aldehyde substrates to alcohols, which in turn are preferred over acids. In each case, resonance stabilization by the phenyl

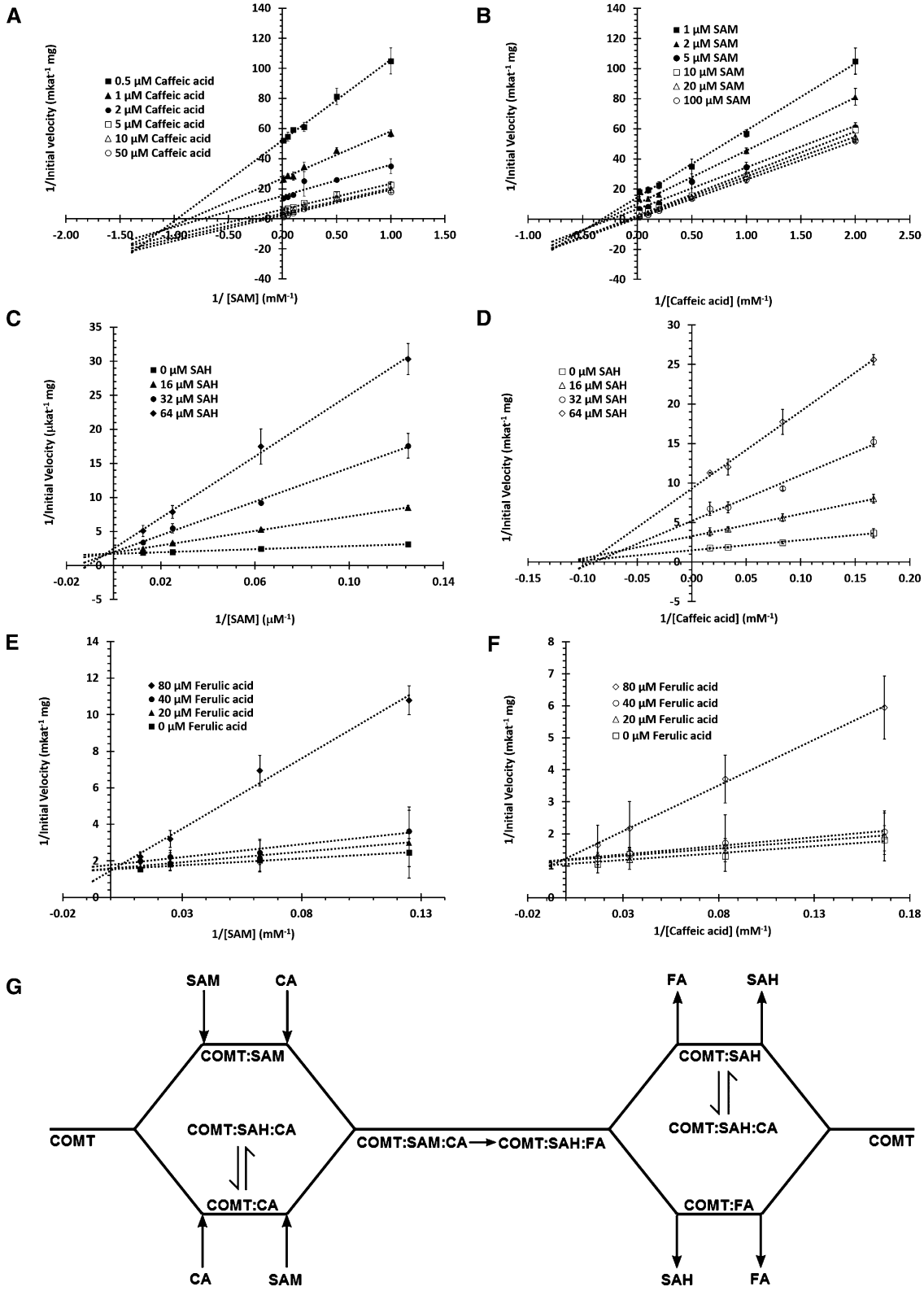

Figure 7. Sequential binding mechanism of SbCOMT. A and B, Lineweaver-Burk plots of SbCOMT activity at various concentrations of caffeic acid with respect to SAM (A) and at various concentrations of SAM with respect to caffeic acid (B). C and D, Lineweaver-Burk plots of SbCOMT activity at varying SAH inhibitory concentrations with respect to SAM (C) and caffeic acid (D). E and F, Lineweaver-Burk plots of SbCOMT activity at varying ferulic acid inhibitory concentrations with respect to SAM (E) and caffeic acid (F). G, Cleland notation of the predicted random bi-bi mechanism of SbCOMT. CA, Caffeic acid; FA, ferulic acid.

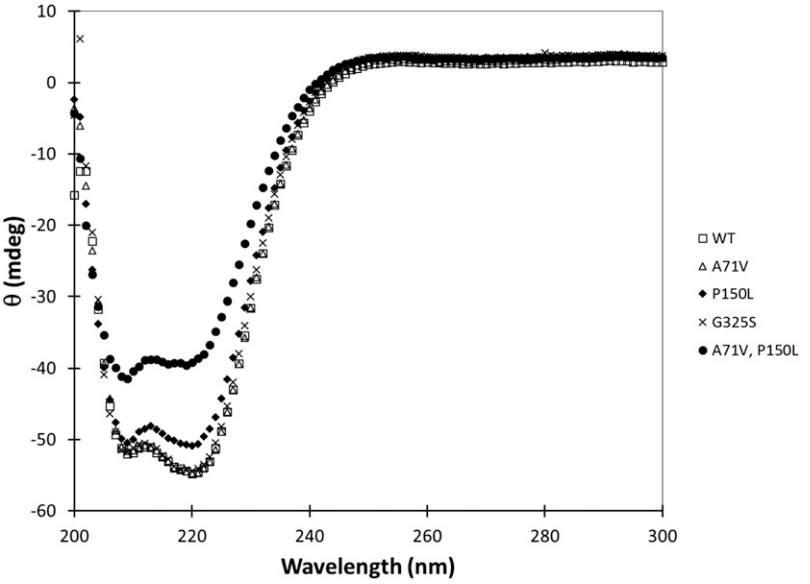

Figure 8. CD spectra for SbCOMT from wild-type sorghum (WT) and *bmr12* mutants. The 200- to 300-nm CD spectra of the wild-type SbCOMT and its four *bmr12* mutants were compared in the same condition (5 μM in phosphate-buffered saline) using an AVIV 202SF spectropolarimeter (AVIV Biomedical) at 25°C. The similar shapes and intensities for the far UV light-CD spectra indicate that wild-type SbCOMT, the A71V mutant, and the G325S mutant contain similar amounts of secondary structure, while the P150L mutant and the A71V, P150L double mutant have reduced secondary structure.

ring of the phenylpropanoids stabilizes the anionic intermediate that results from deprotonation of the 5-hydroxyl phenolic hydrogen (Supplemental Fig. S3). This resonance-stabilized negative charge can be further stabilized by the conjugated aldehyde-propenyl system in the aldehydes, the most favored substrates, by decreasing electron density on the propenyl carbon adjacent to the phenyl ring through inductive withdrawal of electron density. The propenyl system in the alcohols can also stabilize the anionic intermediate by withdrawing electron density away from the propenyl carbon adjacent to the phenyl ring, albeit to a lesser extent than the aldehydes, because the aliphatic alcohol carbon prevents conjugation to the electronegative alcohol oxygen. The acids, which are the least preferred substrates, are unable to stabilize the resonance-stabilized negative charge on the phenyl ring any further because the propenyl system lies adjacent to the carboxylate anion. Shifting electron density away from the resonance-stabilized phenolate toward the carboxylate anion and vice versa would have no net benefit and may be the reason why acids are the least preferred substrates. The acids do react, albeit slowly, and it is expected that COMT active site residues play a role in electrostatic stabilization of the anionic intermediate. In addition, the intrinsic thermodynamic instability of the methylated sulfide in SAM will drive the subsequent transmethylation. With this logic, we predict that 5-hydroxyconiferyl alcohol is a slightly worse substrate than 5-hydroxyconiferaldehyde. It was challenging to test this, due to the ionization source fragmentation of 5-hydroxyconiferyl alcohol during tandem mass spectrometry (MS/MS) characterization.

As shown by our ITC data (Fig. 5C), SbCOMT did not bind caffeoyl-CoA, indicating that there is no overlap in catalytic activity against this compound between COMT and CCoAOMT in sorghum. Although both methyltransferases are probably capable of methylating the 3- and 5-hydroxyl groups, these enzymes are unable to bind both thioester and acidic/aldehydic/alcoholic substrates. Indeed, the loss or reduced activity of COMT in *bmr12* mutants results in a major decrease in S-lignin, whereas G-lignin is relatively unaffected (Bout and Vermerris, 2003; Sattler et al., 2012). This outcome would not be expected if SbCCoAOMT could compensate for most of the lost COMT activity.

Importance of the 4-Hydroxyl Group

A water-mediated hydrogen bond between the 4-hydroxyl group of sinapaldehyde and the Asn-323 side chain Oδ exists in the ternary complex structure of LpCOMT (Louie et al., 2010), which underwent a substantial conformational change compared with Asn-323 found in the SbCOMT SAM complex; thus, the entropic cost of such binding is expected to be high (Table II). Considering that the ITC data for cinnamic acid and cinnamaldehyde (Fig. 5, C and D) indicate no binding of these compounds to COMT, and the lack of inhibitory capacity of cinnamic acid (data not shown), the 4-hydroxyl group is critical for substrate binding.

The Impact of Three *bmr12* Mutations on the Enzyme Activity of SbCOMT

In sorghum, maize, and pearl millet (*Pennisetum glaucum*), *brown midrib* mutations have been shown to reduce lignin content and alter lignin subunit composition (Saballos et al., 2008; Sattler et al., 2010). Four missense *bmr12* mutants were isolated from an ethyl methanesulfonate-mutagenized Targeting Induced Local

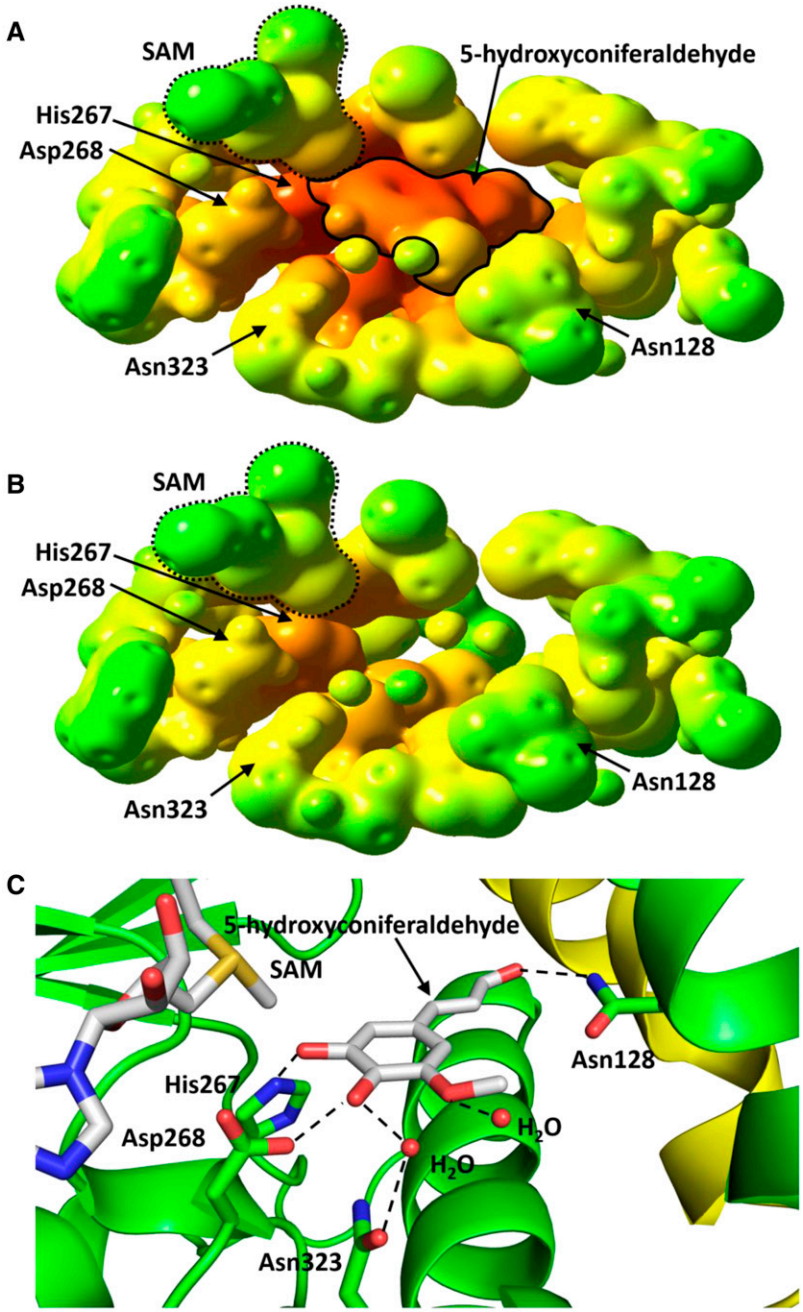

Figure 9. SbCOMT active-site electrostatic potential surface with modeled 5-hydroxyconiferaldehyde and hydrogen bonding interactions. A and B, In A (with 5-hydroxyconiferaldehyde) and B (apo), the modeled active-site amides (Asn-128 and Asn-323) are present as propanamide, Asp-268 is present as propanoate, Glu-296 and Glu-328 are present as acetate, Met-317 is present as ethyl methyl sulfide, and SAM is present as diethylmethylsulfonium. The active site is mapped at an iso value of 0.020 electrons $Bohr^{-3}$ and shown on a potential scale of -3.10×10^{1} Hartrees (red) to +4.00 Hartrees (blue). These images were generated using GaussView 3.09. C, The modeled active site hydrogen bonding interactions. Hydrogen bonds are shown as black dotted lines. The green cartoon represents the protein forming the active site, and the yellow α-helix corresponds to the dimeric partner's α1. This image was generated using the PyMOL Molecular Graphics System, version 1.3 (Schrödinger).

Lesions in Genomes population (Sattler et al., 2012), which changed evolutionarily conserved amino acids Gly-325Ser (*bmr12-30*), Gly-225Asp (*bmr12-35*), and Ala-71Val and Pro-150Leu together (*bmr12-34* and *bmr12-820*). Three of the four mutants (*bmr12-30*, *bmr12-34*, and *bmr12-820*) displayed a significant reduction in Klason lignin content and altered lignin composition, namely a significantly reduced S-G ratio relative to the wild type. The overall impact of these mutations, however, was less severe than the previously characterized *bmr12* mutants containing *COMT* alleles with premature stop codons (Bout and Vermerris, 2003; Saballos et al., 2008; Sattler et al., 2012). In addition, the enzymatic saccharification of pretreated biomass from these same three *bmr12* mutants yielded more Glc relative to the wild type (Sattler et al., 2012). The *bmr12-35* mutant, in which a Gly-225Asp change had occurred, has been proven to be severely misfolded and insoluble. An enzyme assay performed with a mutant protein containing just the Ala-71Val substitution, and using 3,4-dihydroxy-5-methoxybenzaldehyde (a substrate analog mimicking 5-hydroxyconiferylaldehyde), showed that it displayed 82% of wild-type activity. In contrast, Pro-150Leu (by itself) and Gly-325Ser had only 0.1% and 1.2% of wild-type activity, respectively. The combination of Ala-71Val:Pro-150Leu together, which

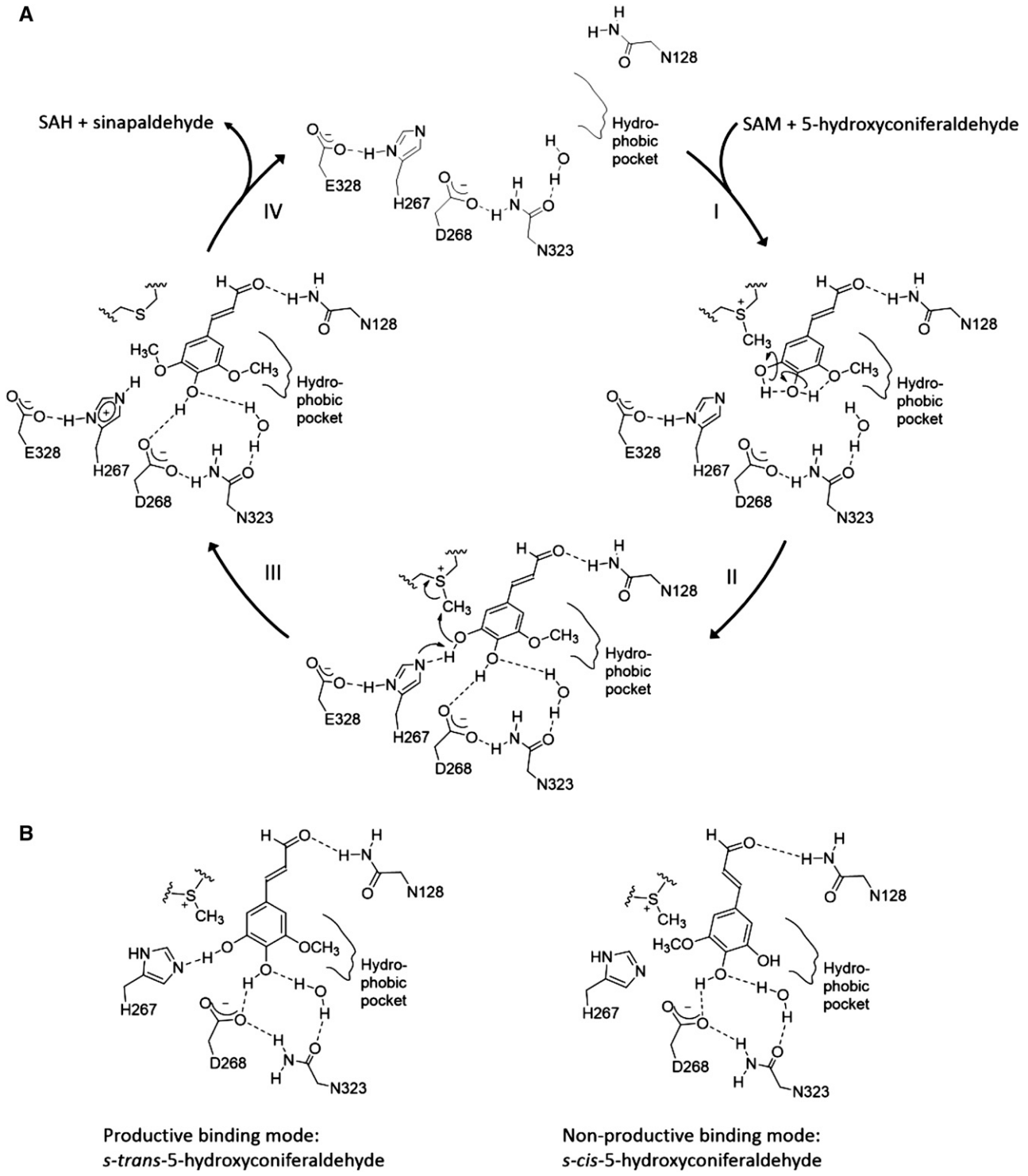

Figure 10. Catalytic mechanism and productive versus nonproductive substrate binding. A, I, 5-Hydroxyconiferaldehyde and SAM bind to the active site with a concomitant release of solvent and active-site closure. Asp-268 aids in reorienting the 4- and 5-hydroxyl groups from the *syn*-conformation favored by the phenylpropanoid molecule to the *anti*-like configuration required for catalysis. II, His-267 abstracts a proton from the 4-hydroxyl group, which is then methylated by SAM. III, SAH and sinapaldehyde product complex prior to COMT reopening. IV, SAH and sinapaldehyde leave, and the basic form of His-267 is regenerated by losing its acidic proton to solvent. B, Productive binding by *S*-trans-5-hydroxyconiferaldehyde (left) and nonproductive binding by *S*-cis-5-hydroxyconiferaldehyde. The positions of the 3-methoxyl and 5-hydroxyl groups of *S*-cis-5-hydroxyconiferaldehyde are switched in the binding site so that the methoxy group is oriented toward His-267 and SAM.

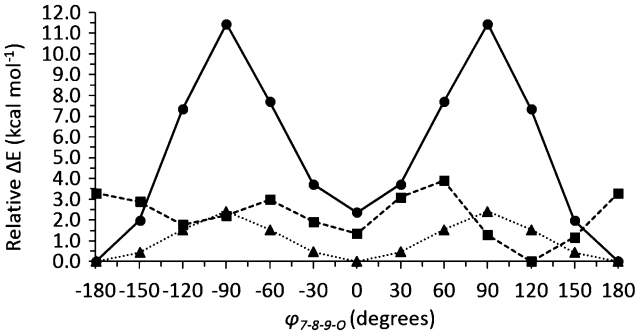

Figure 11. A 360° 5-hydroxyconiferyl substrate $\phi_{7\text{-}8\text{-}9\text{-}O}$ dihedral angle potential energy surface. The $\phi_{7\text{-}8\text{-}9\text{-}O}$ dihedral angle potential energy surface scans are from 5-hydroxyconiferaldehyde (solid lines), 5-hydroxyconiferyl alcohol (dashed lines), and 5-hydroxyferulate (dotted lines) with gas-phase energies for each molecule set relative to their lowest-energy $\phi_{7\text{-}8\text{-}9\text{-}O}$ dihedral angle of 180° for 5-hydroxyconiferaldehyde, 119.94° for 5-hydroxyconiferyl alcohol, and 180° for 5-hydroxyferulate. The 30° incremental scan points for 5-hydroxyconiferaldehyde (circles), 5-hydroxyconiferyl alcohol (squares), and 5-hydroxyferulate (triangles) are shown.

occurred in the *bmr12-34* and *bmr12-820* mutants, reduced enzymatic activity approximately 4,000-fold compared with the wild type (Sattler et al., 2012).

The comparison of secondary structure contents among the wild type and *bmr* mutants via CD spectroscopy revealed that Ala-71Val and Gly-325Ser mutants had the same overall secondary structure when compared with the wild type (Fig. 8). The two mutants containing the Pro-150Leu substitution, however, displayed an increase in random coils, as evidenced by the increase in the 208-nm peak and the shallowness of the 220-nm peak (Fig. 8). This observed decrease in secondary structure contents was most pronounced in the *bmr12-34* mutant Pro-150Leu: Ala-71Val. Pro-150 is located at the beginning of the aforementioned SbCOMT hinge region, an area where the largest differences in backbone dihedral angles between open and closed conformations occurred. A Pro residue often serves as a hinge, in which a simple conformational change from a cis- to a trans-position leads to drastic conformational changes (Kempf et al., 2007). Additionally, the rigidity that a Pro residue imparts to these catalytic hinges has been shown to be essential in maintaining the stability of the mobile loop as well as inducing proper catalytic conformation (Kempf et al., 2007). Thus, replacing Pro in the hinge with Leu could result in drastically reduced catalytic efficiency (Sattler et al., 2012). Finally, the synergistic effect of an additional Ala-71Val mutation may be due to the contribution from the hinge to the dimer interface. The Ala-71 residue is located in the dimer interface, and Ala-71Val did not produce any noticeable effect on the local secondary structure alone, as evidenced in its CD pattern. However, together with the destabilization of the dimer interface enacted by the Pro-150Leu mutation of the adjacent and contributing hinge, Ala-71Val may compound the disorder of the dimer interface and adjacent helices.

CONCLUSION

The combined results from the experiments aimed at characterizing SbCOMT indicate that, in sorghum, this enzyme can catalyze the methylation of the 3-hydroxyl group of caffeic acid and the 5-hydroxyl group of 5-hydroxyconiferaldehyde, and that based on modeling, 5-hydroxyconiferyl alcohol is expected to be an effective substrate. Given that the addition of the 3-hydroxyl group occurs at the level of the CoA ester, by the action of HCT and *p*-coumaroyl ester 3′-hydroxylase, and that neither caffeoyl-CoA nor caffeyl alcohol is an effective substrate for SbCOMT, the primary role of SbCOMT is in the biosynthesis of sinapaldehyde and sinapyl alcohol, which, following polymerization, appear as syringyl units in the lignin. This role of SbCOMT is supported by the decrease in the S-G ratio in *bmr12* mutants. Given the similarities in phenotype observed in maize, sugarcane, and switchgrass with down-regulated *COMT* genes, the observations on transgenic ryegrass do not appear to represent a metabolic pathway shared by grasses in general.

A key challenge in the development of next-generation bioenergy sorghums is the balance between agroindustrial needs (enhanced yields of fermentable sugars following enzymatic saccharification) and plant fitness during the growing season (resistance to lodging, insects, and fungi). These additional *bmr12* mutants represent new tools to decrease lignin content and S-G ratio and enable the degree to which cell wall composition in the bioenergy grass sorghum is modified using nontransgenic approaches. A more detailed understanding of how COMT functions as a result of the studies described here will provide additional tools to tailor cell wall composition by providing targets for mutations that can be identified in natural or mutagenized populations through reverse genetics approaches or that can be introduced using genome-editing tools such as TALEN technology. This technology relies on fusion proteins consisting of transcription activator-like (TAL) effectors of plant pathogenic *Xanthomonas* spp. to the *Fok*I endonuclease (EN; Cermak et al., 2011). The binding specificity of TALENs is determined by customizable arrays of polymorphic amino acid repeats in the TAL effectors, so that specific sites in the genome can be cleaved and modified with the help of the cell's repair machinery. An additional strategy involving a transgenic approach (pending a reliable mechanism to control gene flow) is the introduction of a custom-designed *COMT* gene in the *bmr12-ref* mutant, which does not contain a functional copy of this gene (Bout and Vermerris, 2003; Sattler et al., 2012).

MATERIALS AND METHODS

Chemicals

Chemicals were obtained from Sigma-Aldrich and Fisher Scientific. Solutions for the crystallization screens were obtained from Hampton Research. 5-Hydroxyconiferaldehyde was synthesized from 5-hydroxyvanillin by first acetylating it with acetic anhydride-pyridine to give acetylated 5-hydroxyvanillin, which was then reacted with triethyl phosphonoacetate and sodium hydride in dry tetrahydrofuran to yield acetylated ethyl 5-hydroxyferulate. The ester was reduced by diisobutylaluminum hydride in toluene to give 5-hydroxyconiferyl alcohol, followed by *tert*-butyldimethylsilylation with *tert*-butyldimethylsilyl triflate and pyridine in ethyl acetate. This *tert*-butyldimethylsilyl ether was oxidized by 2,3-dichloro-5,6-dicyanobenzoquinone in dioxane to afford 5-hydroxyconiferaldehyde *tert*-butyldimethylsilyl ether, from which the silyl ether group was hydrolyzed by NaOH in aqueous dioxane to produce 5-hydroxyconiferaldehyde, the structure of which was confirmed by NMR (Osakabe et al., 1999).

Recombinant Enzyme Expression and Purification

SbCOMT from sorghum (*Sorghum bicolor*; *Bmr12*; Sb07g003860), both wild-type and mutated proteins, which corresponded to *bmr12* missense mutations described previously (Sattler et al., 2012), were expressed in a strain of *E. coli* [Rosetta(DE3)pLysS] cells and induced with 0.5 mM isopropyl β-D-1-thio-galactopyranoside at 20°C for 12 h. Harvested cells were sonicated in lysis buffer (50 mM Tris, 300 mM NaCl, and 15 mM imidazole, pH 8). SbCOMT bound to nickel-nitrilotriacetic acid agarose resin (Bio-Rad) and was washed with 10 column volumes of lysis buffer and then eluted with elution buffer (50 mM Tris, 300 mM NaCl, and 250 mM imidazole, pH 8). The eluted fractions were pooled and buffer exchanged into 20 mM Tris and 2 mM dithiothreitol, pH 7.5. The final purification was performed through a MonoQ10/100GL (GE Healthcare) column with a linear gradient up to 2 M NaCl. The 200 mM NaCl fraction, where SbCOMT was detected, was collected, pooled, and buffer exchanged into 20 mM Tris, 150 mM NaCl, and 2 mM dithiothreitol, pH 7.5. The final protein concentration was determined via bicinchoninic acid assay (Pierce), and pure SbCOMT enzymes were stored at 4°C for crystallization or −20°C for prolonged storage.

Crystallization and Structure Determination

Apo-form SbCOMT at 15 mg mL^{-1} crystallized in 0.03 M citric acid, 7 mM Bis-Tris propane, and 20% (w/v) polyethylene glycol 3,350, pH 7.6. The SAM binary complex crystallized in 0.2 M $MgCl_2$, 0.1 M Tris, 25% (w/v) polyethylene glycol 3,350, pH 8.5, with 20 mg mL^{-1} SbCOMT preequilibrated with SAM solution (1 mM). Crystals were obtained using the hanging drop vapor-diffusion method and typically appeared within 3 weeks. All diffraction data were collected at the Berkeley Advanced Light Source (beamline 8.2.1) and were processed and scaled with the HKL2000 package (Otwinowski and Minor, 1997). Initial phasing of apo-form COMT diffraction data was performed via molecular replacement in PHENIX (Adams et al., 2002) using the coordinates of COMT from ryegrass (*Lolium perenne*; PDB identifier 3P9C; Louie et al., 2010). Iterative model building and refinement took place using the programs COOT (Emsley et al., 2010) and PHENIX. The SAM binary complex structure of SbCOMT was solved via molecular replacement using the apo-form model of SbCOMT as initial coordinates. Coordinates of apo-COMT and SAM complex COMT have been deposited in the PDB. X-ray diffraction and refinement statistics are listed in Table I.

ITC and CD Spectroscopy

ITC measurements were carried out in a VP-ITC instrument (MicroCal) as described previously (Green et al., 2012), with the exception that enzyme concentration was 50 μM and the buffer used was 50 mM sodium phosphate, pH 6.5. CD spectra for both wild-type and mutant SbCOMT enzymes were measured between 200 and 300 nm using an AVIV 202SF spectropolarimeter (AVIV Biomedical) at 25°C, at a concentration of 5 μM, in phosphate-buffered saline.

Enzymatic Activity Assays of SbCOMT

All kinetic assays were performed in triplicate in 50 mM sodium phosphate buffer, pH 6.5. 5-Hydroxyconiferaldehyde concentrations were varied from 0 to 5 μM, and the concentrations of SAM and wild-type SbCOMT were fixed at 300 and 1.3 μM, respectively. Reactions were carried out for 30 s at room temperature and quenched with 1 M formic acid and 10 μM sinapic acid. The kinetic assays for caffeic acid and SAM were carried out for 20 s at room temperature with a concentration of 13 μM wild-type SbCOMT, due to the lower turnover rate of caffeic acid and HPLC-MS/MS detection limits. Concentrations of caffeic acid were varied from 0 to 200 μM, with a constant concentration of SAM at 300 μM. The concentrations of SAM were varied from 0 to 500 mM, with a constant concentration of 150 μM caffeic acid. For product inhibition assays, the concentration of the substrate not being tested was held at its K_m, while the concentration of the substrate being tested was varied from 0.5 to 5 K_m. The product of interest was varied at 0, 2, and 4 K_{iapp} (for apparent inhibition constant).

HPLC-MS/MS

Samples were analyzed using a series 1100 HPLC system (Agilent Technologies) coupled to an API 4000 tandem mass spectrometer (Applied Biosystems/MDS Sciex) with a turbospray electrospray ionization source. Analytes were detected in negative ion multiple reaction mode. Chromatography was performed on a Zorbax Eclipse XDB-C8 column (4.6 × 150 mm, 5 μM; Agilent). Mobile phase A was composed of 0.05% (v/v) formic acid and 0.2% (v/v) acetic acid in water, while mobile phase B was 90% (v/v) acetonitrile and 0.1% (v/v) formic acid in water.

Quantitation of Ferulic Acid

The column was equilibrated at initial conditions of 99% mobile phase A at a 1,000 μL min^{-1} flow rate for 2.5 min. Chromatographic separation was achieved using a linear gradient over the next 4 min to 5% mobile phase A and was held at 5% A for 1 min. Over the next 1 min, mobile phase A was ramped back to 99% and then held constant for a reequilibration time of 1 min. The total chromatographic assay time was 8 min per sample, and the retention times for ferulic acid and the sinapic acid internal standard were 5 and 4.8 min, respectively. The multiple reaction monitoring mass-to-charge ratio transitions for ferulic acid and sinapic acid were 193.2 → 134.2 and 223.2 → 193.2, respectively. Quantitation was achieved by extrapolating from a standard curve of authentic ferulic acid using a concentration range of 0.09 to 20 μM.

Quantitation of Sinapaldehyde

Using a flow rate of 1,000 μL min^{-1}, the column was equilibrated at initial conditions of 99% mobile phase A for 2.5 min. Chromatographic separation was achieved using a linear gradient over the next 17.5 min to 5% mobile phase A and was held at 5% A for 1 min. Over the next 1 min, mobile phase A was ramped back to 99% and then held constant for a reequilibration time of 3 min. The total chromatographic assay time was 25 min per sample, and the retention times for sinapaldehyde and sinapic acid (internal standard) were 11.1 and 10.2 min, respectively. The multiple reaction mode mass-to-charge ratio transitions monitored for sinapaldehyde and sinapic acid were 193.2 → 177.7 and 223.2 → 193.2, respectively. Quantitation was achieved by extrapolating from a standard curve of authentic sinapaldehyde using a concentration range of 0.09 to 5 μM.

Electrostatic Potential Surface Calculation of SbCOMT Substrates and Substrate-Binding Pocket

Structures for *p*-coumarate, caffeate, 5-hydroxyferulate, and their corresponding aldehydes and alcohols were optimized in Gaussian 09 (Frisch et al., 2009) at the B3LYP level of theory using double-zeta correlation-consistent basis sets (cc-pVDZ) with augmented functions (aug-cc-pVDZ) on carbon and oxygen (Peterson and Dunning, 2002), hereafter denoted as aVDZ. The acids and aldehydes were optimized with a C_7-C_8-C_9-O propenal/propenoate chain 180° dihedral angle. The 180° dihedral angle propenol chain of the alcohols was obtained by performing a relaxed potential energy surface scan and taking the 180° dihedral rotamer as the final structure. Six points $Bohr^{-1}$ electrostatic potential and total electron density grids were generated from the optimized molecular self-consistent field densities by the Gaussian 09 cubegen utility and mapped in GaussView 3.09 (Frisch, 2004) as the electrostatic potential on the electron density at an iso value of 0.001 electrons $Bohr^{-3}$.

The electrostatic potential surface of the modeled SbCOMT phenylpropanoid-binding pocket was determined using a truncated model consisting of SAM, 5-hydroxyconiferaldehyde, Leu-124, Asn-128, Gln-129, Leu-133, Met-177,

Trp-264, His-267, Asp-268, Trp-269, Val-295, Glu-296, Cys-297, Val-312, Val-315, Ile-318, Met-319, His-322, Asn-323, Glu-328, and, from the dimeric partner, Met-21 and Ser-25. A single-point calculation using PM6 semiempirical theory (Stewart, 2007) in Gaussian 09 was performed on the truncated model. The self-consistent field electron density and potentials were generated as stated previously, but at an iso value of 0.020 electrons $Bohr^{-3}$.

Analysis of the Internal Rotational Energy Barrier of 5-Hydroxyconiferylaldehyde/Alcohol/Acid

The C_7-C_8-C_9-O dihedral angles of 5-hydroxyconiferaldehyde, acid, and alcohol were subjected to a relaxed potential energy surface scan of 12 steps at 30° per step at the B3LYP/aVDZ level of theory using tight optimization criteria and an ultrafine integration grid. A frequency calculation on the two minima of 5-hydroxyconiferaldehyde, corresponding to the *S*-cis- and *S*-trans-conformations, was performed at the same level of theory. The resulting free energies were used to calculate the relative populations of *S*-cis-5-hydroxyconiferaldehyde and *S*-trans-5-hydroxyconiferaldehyde at 298.15 K by modeling the *S*-cis and *S*-trans-conformers as a two-state Boltzmann distribution.

Modeling the SAM:5-Hydroxyconiferaldehyde: COMT Complex

Manipulations of dihedral angles of the SAM binary complex of SbCOMT were performed to bring it to the superimposable position with the ternary complex structure of LpCOMT (PDB identifier 3P9I). After changing the superimposed SAH to SAM and sinapaldehyde to 5-hydroxyconiferaldehyde, the resulting SbCOMT structure was optimized in CPU+GPU MOPAC2012 (Maia et al., 2012; Stewart, 2012) using the semiempirical PM7-MOZYME (Stewart, 2009) linear scaling self-consistent field method and a 3 kcal mol^{-1} $Å^{-2}$ movement constraint. This constrained optimization was followed by unconstrained optimization of all residues within 7 Å of the substrates, and finally, conventional PM7 (Stewart, 2013) optimization of those same residues.

Supplemental Data

The following materials are available in the online version of this article.

Supplemental Figure S1. The absolute difference between the Ψ and Φ of 3P9C and 3P9I dihedral angles.

Supplemental Figure S2. Chemical structure of cinnamate, *p*-coumarate, caffeate, 5-hydroxyferulate, cinnamaldehyde, *p*-coumaraldehyde, caffealdehyde, 5-hydroxyconiferaldehyde, cinnamyl alcohol, *p*-coumaryl alcohol, caffeyl alcohol, and 5-hydroxyconiferyl alcohol.

Supplemental Figure S3. Electron delocalization of 5-hydroxyl phenolate anion. Delocalization of the 5-hydroxyl phenolate anion's negative charge upon deprotonation at the 5-hydroxyl group for 5-hydroxyconiferaldehyde, 5-hydroxyconiferyl alcohol, and 5-hydroxyferulate.

ACKNOWLEDGMENTS

We thank Tammy Gries, Yunying Mei, and Christina Bender for technical assistance in the experiments presented here.

Received April 23, 2014; accepted June 17, 2014; published June 19, 2014.

LITERATURE CITED

Adams PD, Grosse-Kunstleve RW, Hung LW, Ioerger TR, McCoy AJ, Moriarty NW, Read RJ, Sacchettini JC, Sauter NK, Terwilliger TC (2002) PHENIX: building new software for automated crystallographic structure determination. Acta Crystallogr D Biol Crystallogr **58:** 1948–1954

Altschul SF, Madden TL, Schäffer AA, Zhang J, Zhang Z, Miller W, Lipman DJ (1997) Gapped BLAST and PSI-BLAST: a new generation of protein database search programs. Nucleic Acids Res **25:** 3389–3402

Atanassova R, Favet N, Martz F, Chabbert B, Tollier M, Monties B, Fritig B, Legrand M (1995) Altered lignin composition in transgenic tobacco expressing *O*-methyltransferase sequences in sense and antisense orientation. Plant J **8:** 465–477

Berlin A, Balakshin M, Gilkes N, Kadla J, Maximenko V, Kubo S, Saddler J (2006) Inhibition of cellulase, xylanase and β-glucosidase activities by softwood lignin preparations. J Biotechnol **125:** 198–209

Bout S, Vermerris W (2003) A candidate-gene approach to clone the sorghum *Brown midrib* gene encoding caffeic acid *O*-methyltransferase. Mol Genet Genomics **269:** 205–214

Cermak T, Doyle EL, Christian M, Wang L, Zhang Y, Schmidt C, Baller JA, Somia NV, Bogdanove AJ, Voytas DF (2011) Efficient design and assembly of custom TALEN and other TAL effector-based constructs for DNA targeting. Nucleic Acids Res **39:** e82

Chabbert B, Tollier M, Monties B, Barriere Y, Argillier O (1994) Biological variability in lignification of maize: expression of the *brown midrib bm3* mutation in three maize cultivars. J Sci Food Agric **64:** 349–355

Chen F, Dixon RA (2007) Lignin modification improves fermentable sugar yields for biofuel production. Nat Biotechnol **25:** 759–761

Dien B, Sarath G, Pedersen J, Sattler S, Chen H, Funnel-Harris D, Nichols N, Cotta M (2009) Improved sugar conversion and ethanol yield for forage sorghum (*Sorghum bicolor* L. Moench) lines with reduced lignin contents. Bioenerg Res **2:** 153–164

Egawa T, Matsumoto R, Yamamotom D, Takahashi H (2008) Molecular structure of trans-cinnamaldehyde as determined by gas electron diffraction aided by DFT calculations. J Mol Struct **892:** 158–162

Emsley P, Lohkamp B, Scott WG, Cowtan K (2010) Features and development of Coot. Acta Crystallogr D Biol Crystallogr **66:** 486–501

Frisch M (2004) GaussView, Version 3. Gaussian, Wallingford, CT

Frisch M, Trucks G, Schlegel H, Scuseria G, Robb M, Cheeseman J, Scalmani G, Barone V, Mennucci B, Petersson G, et al (2009) Gaussian 09, Revision C.01. Gaussian, Wallingford, CT

Fu C, Mielenz JR, Xiao X, Ge Y, Hamilton CY, Rodriguez M Jr, Chen F, Foston M, Ragauskas A, Bouton J, et al (2011) Genetic manipulation of lignin reduces recalcitrance and improves ethanol production from switchgrass. Proc Natl Acad Sci USA **108:** 3803–3808

Green AR, Hayes RP, Xun L, Kang C (2012) Structural understanding of the glutathione-dependent reduction mechanism of glutathionyl-hydroquinone reductases. J Biol Chem **287:** 35838–35848

Guo D, Chen F, Inoue K, Blount JW, Dixon RA (2001) Downregulation of caffeic acid 3-*O*-methyltransferase and caffeoyl CoA 3-*O*-methyltransferase in transgenic alfalfa: impacts on lignin structure and implications for the biosynthesis of G and S lignin. Plant Cell **13:** 73–88

Holm L, Sander C (1993) Protein structure comparison by alignment of distance matrices. J Mol Biol **233:** 123–138

Humphreys JM, Chapple C (2002) Rewriting the lignin roadmap. Curr Opin Plant Biol **5:** 224–229

Humphreys JM, Hemm MR, Chapple C (1999) New routes for lignin biosynthesis defined by biochemical characterization of recombinant ferulate 5-hydroxylase, a multifunctional cytochrome P450-dependent monooxygenase. Proc Natl Acad Sci USA **96:** 10045–10050

Jung JH, Fouad WM, Vermerris W, Gallo M, Altpeter F (2012) RNAi suppression of lignin biosynthesis in sugarcane reduces recalcitrance for biofuel production from lignocellulosic biomass. Plant Biotechnol J **10:** 1067–1076

Jung JH, Vermerris W, Gallo M, Fedenko JR, Erickson JE, Altpeter F (2013) RNA interference suppression of lignin biosynthesis increases fermentable sugar yields for biofuel production from field-grown sugarcane. Plant Biotechnol J **11:** 709–716

Kempf JG, Jung JY, Ragain C, Sampson NS, Loria JP (2007) Dynamic requirements for a functional protein hinge. J Mol Biol **368:** 131–149

Lapierre C, Tollier M, Monties B (1988) Mise en évidence d'un nouveau type d'unité constitutive dans les lignines d'un mutant de maïs *bm3*. CR Acad Sci Paris Ser III **307:** 723–728

Louie GV, Bowman ME, Tu Y, Mouradov A, Spangenberg G, Noel JP (2010) Structure-function analyses of a caffeic acid *O*-methyltransferase from perennial ryegrass reveal the molecular basis for substrate preference. Plant Cell **22:** 4114–4127

Maia J, Urquiza Carvalho G, Mangueira C, Santana S, Cabral L, Rocha G (2012) GPU linear algebra libraries and GPGPU programming for accelerating MOPAC semiempirical quantum chemistry calculations. J Chem Theory Comput **8:** 3072–3081

Marita JM, Vermerris W, Ralph J, Hatfield RD (2003) Variations in the cell wall composition of maize *brown midrib* mutants. J Agric Food Chem **51:** 1313–1321

Martz F, Maury S, Pinçon G, Legrand M (1998) cDNA cloning, substrate specificity and expression study of tobacco caffeoyl-CoA 3-*O*-methyltransferase, a lignin biosynthetic enzyme. Plant Mol Biol **36:** 427–437

Meng H, Campbell WH (1998) Substrate profiles and expression of caffeoyl coenzyme A and caffeic acid *O*-methyltransferases in secondary xylem of aspen during seasonal development. Plant Mol Biol **38:** 513–520

Meyer K, Cusumano JC, Somerville C, Chapple CC (1996) Ferulate-5-hydroxylase from Arabidopsis thaliana defines a new family of cytochrome P450-dependent monooxygenases. Proc Natl Acad Sci USA **93:** 6869–6874

Meyer K, Shirley AM, Cusumano JC, Bell-Lelong DA, Chapple C (1998) Lignin monomer composition is determined by the expression of a cytochrome P450-dependent monooxygenase in *Arabidopsis*. Proc Natl Acad Sci USA **95:** 6619–6623

Morreel K, Ralph J, Lu F, Goeminne G, Busson R, Herdewijn P, Goeman JL, Van der Eycken J, Boerjan W, Messens E (2004) Phenolic profiling of caffeic acid O-methyltransferase-deficient poplar reveals novel benzodioxane oligolignols. Plant Physiol **136:** 4023–4036

Osakabe K, Tsao CC, Li L, Popko JL, Umezawa T, Carraway DT, Smeltzer RH, Joshi CP, Chiang VL (1999) Coniferyl aldehyde 5-hydroxylation and methylation direct syringyl lignin biosynthesis in angiosperms. Proc Natl Acad Sci USA **96:** 8955–8960

Otwinowski Z, Minor W (1997) Processing of x-ray diffraction data collected in oscillation mode. Methods Enzymol **276:** 307–326

Palmer NA, Sattler SE, Saathoff AJ, Funnell D, Pedersen JF, Sarath G (2008) Genetic background impacts soluble and cell wall-bound aromatics in *brown midrib* mutants of sorghum. Planta **229:** 115–127

Parvathi K, Chen F, Guo D, Blount JW, Dixon RA (2001) Substrate preferences of *O*-methyltransferases in alfalfa suggest new pathways for 3-*O*-methylation of monolignols. Plant J **25:** 193–202

Paterson AH, Bowers JE, Bruggmann R, Dubchak I, Grimwood J, Gundlach H, Haberer G, Hellsten U, Mitros T, Poliakov A, et al (2009) The *Sorghum bicolor* genome and the diversification of grasses. Nature **457:** 551–556

Pedersen J, Toy J, Funnell D, Sattler S, Oliver A, Grant R (2008) Registration of BN611, AN612, BN612, and RN613 Sorghum genetic stocks with stacked *bmr-6* and *bmr-12* genes. Journal of Plant Registrations **2:** 258–262

Peterson K, Dunning T (2002) Accurate correlation consistent basis sets for molecular core-valence correlation effects: the second row atoms Al-Ar, and the first row atoms B-Ne revisited. J Chem Phys **117:** 10548–10560

Propheter J, Staggenborg S (2010) Performance of annual and perennial biofuel crops: nutrient removal during the first two years. Agron J **102:** 798–805

Ralph J, Lapierre C, Marita JM, Kim H, Lu F, Hatfield RD, Ralph S, Chapple C, Franke R, Hemm MR, et al (2001) Elucidation of new structures in lignins of CAD- and COMT-deficient plants by NMR. Phytochemistry **57:** 993–1003

Ralph J, Lundquist K, Brunow G, Lu F, Kim H, Schatz P, Marita J, Hatfield R, Ralph S, Christensen J, et al (2004) Lignins: natural polymers from oxidative coupling of 4-hydroxyphenylpropanoids. Phytochem Rev **3:** 29–60

Saballos A, Vermerris W, Rivera L, Ejeta G (2008) Allelic association, chemical characterization and saccharification properties of *brown midrib* mutants of sorghum (*Sorghum bicolor* (L.) Moench). Bioenerg Res **1:** 193–204

Sarath G, Mitchell RB, Sattler SE, Funnell D, Pedersen JF, Graybosch RA, Vogel KP (2008) Opportunities and roadblocks in utilizing forages and small grains for liquid fuels. J Ind Microbiol Biotechnol **35:** 343–354

Sattler S, Funnell-Harris D, Pedersen J (2010) *Brown midrib* mutations and their importance to the utilization of maize, sorghum, and pearl millet lignocellulosic tissues. Plant Sci **178:** 229–238

Sattler S, Palmer N, Saballos A, Greene A, Xin Z, Sarath G, Vermerris W, Pedersen J (2012) Identification and characterization of four missense mutations in *Brown midrib12* (*Bmr12*), the caffeic acid *O*-methyltransferase (COMT) of sorghum. Bioenerg Res **5:** 855–865

Shadle G, Chen F, Srinivasa Reddy MS, Jackson L, Nakashima J, Dixon RA (2007) Down-regulation of hydroxycinnamoyl CoA: Shikimate hydroxycinnamoyl transferase in transgenic alfalfa affects lignification, development and forage quality. Phytochem **68:** 1521–1529

Stewart JJ (2007) Optimization of parameters for semiempirical methods. V. Modification of NDDO approximations and application to 70 elements. J Mol Model **13:** 1173–1213

Stewart JJ (2009) Application of the PM6 method to modeling proteins. J Mol Model **15:** 765–805

Stewart J (2012) MOPAC2012. Stewart Computational Chemistry, Colorado Springs, CO

Stewart JJ (2013) Optimization of parameters for semiempirical methods. VI. More modifications to the NDDO approximations and re-optimization of parameters. J Mol Model **19:** 1–32

Tu Y, Rochfort S, Liu Z, Ran Y, Griffith M, Badenhorst P, Louie GV, Bowman ME, Smith KF, Noel JP, et al (2010) Functional analyses of caffeic acid *O*-methyltransferase and cinnamoyl-CoA-reductase genes from perennial ryegrass (*Lolium perenne*). Plant Cell **22:** 3357–3373

Van Doorsselaere J, Baucher M, Chognot E, Chabbert B, Tollier M, Petit-Conil M, Leplé J, Pilate G, Cornu D, Monties B, et al (1995) A novel lignin in poplar trees with a reduced caffeic acid/5-hydroxyferulic acid *O*-methyltransferase activity. Plant J **8:** 855–864

Vanholme R, Demedts B, Morreel K, Ralph J, Boerjan W (2010) Lignin biosynthesis and structure. Plant Physiol **153:** 895–905

Vanholme R, Morreel K, Ralph J, Boerjan W (2008) Lignin engineering. Curr Opin Plant Biol **11:** 278–285

Vermerris W, Saballos A (2012) Genetic enhancement of sorghum for biomass utilization. *In* A Paterson, ed, Genetics and Genomics of the Saccharinae. Springer, New York, pp 391–428

Vermerris W, Saballos A, Ejeta G, Mosier N, Ladisch M, Carpita N (2007) Molecular breeding to enhance ethanol production from corn and sorghum stover. Crop Sci **47:** S142–S153

Vermerris W, Sherman DM, McIntyre LM (2010) Phenotypic plasticity in cell walls of maize *brown midrib* mutants is limited by lignin composition. J Exp Bot **61:** 2479–2490

Wagner A, Tobimatsu Y, Phillips L, Flint H, Torr K, Donaldson L, Pears L, Ralph J (2011) CCoAOMT suppression modifies lignin composition in *Pinus radiata*. Plant J **67:** 119–129

Walker A, Hayes R, Youn B, Vermerris W, Sattler S, Kang C (2013) Elucidation of the structure and reaction mechanism of sorghum hydroxycinnamoyltransferase and its structural relationship to other coenzyme A-dependent transferases and synthases. Plant Physiol **162:** 640–651

Wortmann CS, Regassa T (2011) Sweet sorghum as a bioenergy crop for the US Great Plains. In M Aurelio Dos Santos Bernardes, ed, Economic Effects of Biofuel Production, InTech, pp 225–240 http://www.intechopen.com/books/economic-effects-of-biofuelproduction/sweet-sorghum-as-a-bioenergy-crop-for-the-us-great-plains

Ximenes E, Kim Y, Mosier N, Dien B, Ladisch M (2010) Inhibition of cellulases by phenols. Enzyme Microb Technol **46:** 170–176

Zubieta C, Kota P, Ferrer JL, Dixon RA, Noel JP (2002) Structural basis for the modulation of lignin monomer methylation by caffeic acid/5-hydroxyferulic acid 3/5-*O*-methyltransferase. Plant Cell **14:** 1265–1277